Spatial Distribution of High-Energy Electron Emission from Water Plasmas Produced by Femtosecond Laser Pulses

Y.T. Li,[1] J. Zhang,[1,*] Z.M. Sheng,[1] H. Teng,[1] T.J. Liang,[2] X.Y. Peng,[1] X. Lu,[1] Y.J. Li,[1] and X.W. Tang[2]
[1]*Laboratory of Optical Physics, Institute of Physics, Chinese Academy of Sciences, Beijing 100080, People's Republic of China*
[2]*Institute of High Energy Physics, Chinese Academy of Sciences, Beijing 100039, People's Republic of China*
(Received 24 January 2002; published 25 April 2003)

High energy electrons emitted by water plasmas produced by a single or a multiple laser pulse are investigated. The multipulse mode greatly enhances the generation and the temperature of hot electrons. Directional emission of high energy electrons over 25 keV is observed in two symmetric directions with respect to the laser axis and at 46° from the directions of the laser electric field. Two-dimensional particle-in-cell simulations reproduce well the experimental results and indicate that the acceleration mechanism of the high energy electrons is due mainly to the resonance absorption at the edge of the spherical droplets formed by the leading pulse.

DOI: 10.1103/PhysRevLett.90.165002 PACS numbers: 52.38.–r, 52.38.Kd, 52.50.Jm

Research during the past decades on laser-produced liquid plasmas has mainly concentrated on x-ray emission from liquid jet [1], laser-induced breakdowns resulting from focusing a long laser (nanosecond or subnanosecond) pulse inside a liquid [2,3]. More recently, there has also been research on single cavitation bubble luminescence in liquids [4,5]. However, many practical applications such as laser surgery, etc. [6] involve the interaction of a laser beam with an air-liquid interface instead of inside a liquid. In this Letter, we study the high energy electron emission from water plasmas produced by focusing femtosecond laser pulses on the water surface. We find that the spatial distribution of the hot electrons is very different from the behavior of hot electrons emitted from the interactions of ultrashort laser pulses with solids, gases, and clusters.

The experiments are carried out on an ultrashort-pulse laser facility (5 mJ, 150 fs, 800 nm, and 10 Hz). Figure 1 shows the experimental setup. The laser beam is focused by an f/4 spherical lens onto the air-liquid surface of distilled water, forming a focal spot with a diameter of $\sim 10\ \mu$m. One can produce a single pulse or a multiple pulse train by adjusting the Pockels cell in the laser chain. The inset in Fig. 1 shows the shape of the multipulse measured by a Tektronix TDS 520A digital oscilloscope. The separation time between two pulses in the multipulse is 10 ns. The peak intensity on the target surface is about 1×10^{16} W/cm^2 for the single pulse case.

The hot electrons are recorded by LiF (Mg, Cu, P) thermoluminescence dosimeters (TLDs) with a 6-μm-thick aluminum filter. The dimension of the LiF detector is 4.5 mm diam $\times$ 0.8 mm. The space over the laser focus is covered by more than 100 TLDs mounted on a 2π spherical shell. A hole is left on the top of the hemispheric bracket for the incident laser beam. A rotatable reflection mirror, M2, converts the horizontal laser beam to vertical or obliquely incident on the water surface. The angular resolution of this system is about 6°. LiF is sensitive to ions, x-ray photons, and electrons. However, the long distance in air and aluminum filter are the natural filters for the ions generated in the experiment. Comparison of the dosages at the TLDs with and without a 1500 G magnetic field shows that the contribution of x rays is 20 times lower than that of electrons. Thus, the dosage recorded by the TLDs is contributed mainly by the hot electrons.

A γ-ray spectrometer is used to measure the x-ray bremsstrahlung [7]. The plasma expansion is probed by splitting a small portion of the laser beam from the main beam and passing it parallel across the plasma after frequency doubling to 400 nm.

Figure 2 shows the x-ray spectra for the single and multiple laser pulse cases, respectively. The spectra are obtained by the γ-ray spectrometer, viewing the plasma at 80° with respect to the target normal. The laser pulses

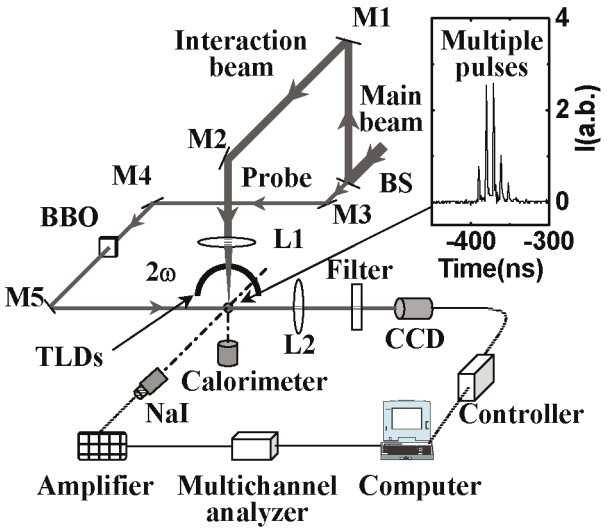

FIG. 1 (color online). The experimental layout. M1–M5 are reflection mirrors and BS represents the beam splitter.

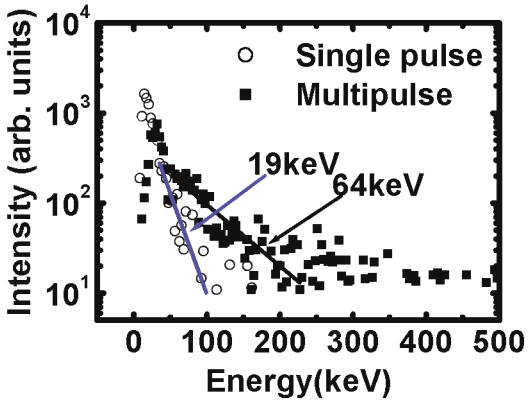

FIG. 2 (color online). Comparison of the hard x-ray spectra emitted from laser-water plasmas produced by a single pulse and a multipulse train.

are incident on the water surface normally. Compared with the case of the single pulse, the multiple pulse train greatly enhances the emission of x rays. The maximum photon energy exceeds 300 keV, and the effective temperature of the hot electrons is up to 64 keV by fitting an $\exp(-E/kT)$ to the tail of the photon distribution. This temperature is comparable to the values in the laser-solid interaction under similar experimental conditions [8].

Figure 3(a) displays the spatial distribution of electrons with energies higher than 25 keV produced by multiple pulses at the normal incidence. The dose is accumulated over 10 000 shots. A striking aspect is the presence of two distinct peaks, symmetric with respect to the laser incident direction, in the plane formed by the electric vector and the propagation vector. The direction of the two peaks is at 46° backward from the electric vector with a full width at half-maximum (FWHM) (Gaussian profile) of 34°. When the plane of the laser polarization is rotated by 90° using a $\lambda/2$ wave plate, the direction of the electron emission is found to rotate by 90° correspondingly, as shown in Fig. 3(b). The solid line and the square points in Fig. 3(c) show the angular distribution of electrons on the chord through the electron jets obtained from Fig. 3(a), where 0° corresponds to the laser propagation axis and 90° and 270° correspond to the direction of the electric vector. Assuming the electrons are subjected to a Maxwellian distribution with an effective temperature of 64 keV (deduced from the hard x-ray spectrum), we estimate the total number of electrons is 2×10^5/sr per shot in the jets using the ITS 3.0 code (Integrated TIGER Series of Coupled Electron/Photon) [9].

When the p-polarized laser pulses are incident at 20° with respect to the target normal, two peaks of hot electron emission are again found. The latter retains the axial symmetry with respect to the laser propagation vector in the plane of polarization. When s-polarized laser beams are used at an incident angle of 20°, the two peaks of hot electrons also rotate by 90°. Note that the results here are quite different from those observed in corresponding laser-solid plasma interactions [8].

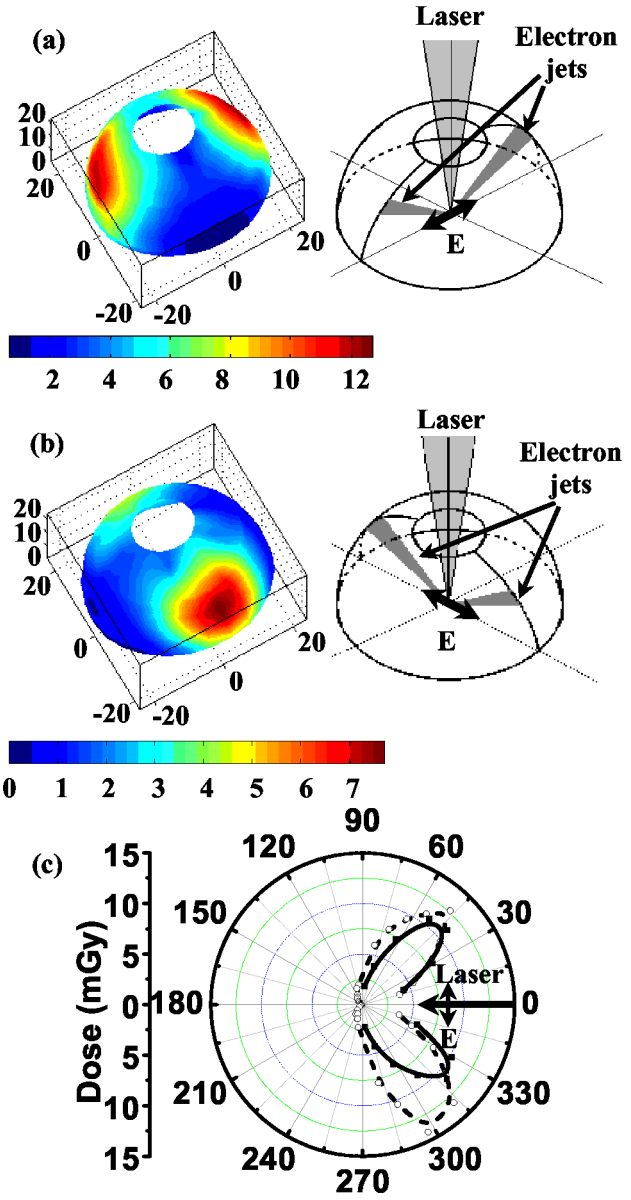

FIG. 3 (color online). (a) Spatial distribution of hot electrons with energies > 25 keV at the normal incidence. (b) The plane of the polarization rotated by 90°, the two electron peaks are rotated correspondingly. Angular distribution on the chord through the electron jets obtained from (a) (solid line and squares) and angular distribution of the hot electrons emitted from the direct laser-water droplets interaction (dashed line and circles) are shown in (c).

We have also investigated hot electrons generated by a single pulse, but the dosage recorded by the TLDs is only slightly higher than that of the background. This is expected because the average temperature of the hot electrons is only 19 keV (see Fig. 2), and most of them cannot penetrate the 6-μm-thick aluminum filter in front of the TLDs. For comparison, a prepulse with a very short separation time of 50 ps is introduced in some shots. We find that the effect of such a short separation time is

negligible. It is of interest to compare the case of interaction with solid targets, where such a prepulse would dramatically enhance the production of hot electrons [7].

To understand the characteristics of the plasma produced by the leading pulse in the multipulse mode, we model the interaction using a 1D hydrodynamic simulation code (MED103) [10]. We find that a very cool preplasma with temperature <0.1 eV and low-density gradient is formed at 10 ns. Thus, more energy of the following laser pulses can be deposited in the interaction region [11]. The energy of the forward scattered light for both single and multiple pulses is measured in our experiment by an energy calorimeter and we find that energy absorption is more efficient in the multipulse mode. However, this higher energy deposition cannot fully explain the behavior of the hot electrons observed.

To clarify the effects of the leading pulse on the interaction, the plasma is diagnosed by the optical shadowgraphy. Typical shadowgrams of the backward expansion into air and the forward expansion into water of the water plasma produced by a single laser pulse are shown in Fig. 4. The shadowgrams are recorded at a delay time of 10 ns, the same time as the separation time in the multipulse mode. The filaments in water are caused by the leakage of the laser beam. A shock wave into air and a density cavity (or crater) into water are simultaneously produced by the plasma pressure. When the second pulse arrives after 10 ns, both the shock wave front in air and the bottom of the water crater have moved away, ~ 150 and ~ 110 μm from the focus, respectively. Most of the preplasma produced by the first pulse will recombine after 10 ns. Therefore, the possible candidates to be interacted with by the following pulses are (a) the spherical critical density surface at the bottom of the water crater; (b) the compressed ambient air and the water vapor wrapped between the shock wave and the concave water surface (these gases may be partially ionized); and (c) the water droplets from the condensation of water vapor or from the direct explosive emission from the focus. A simple interaction model is illustrated in Fig. 4(c). Next we find out which one is responsible for the experimental results and how the hot electrons are produced.

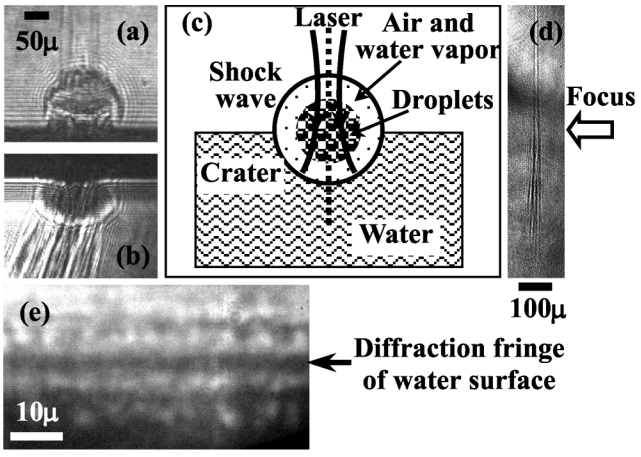

FIG. 4. (a) Shadowgrams of the backward expansion in air at the normal incidence; (b) the forward density cavitation in the water at the oblique incidence; (c) schematic showing the interaction model; (d) self-focusing and defocusing of a single pulse taken at 1 ns; and (e) a typical image showing the droplets above the water surface.

One might think that the generation of hot electrons is related to the resonance absorption on the spherical critical surface of the water crater or on a backward propagating critical density ionization front produced by the first pulse. The following laser beam effectively defocused by the air breakdown would meet two parts of the surface that are at the correct angle for the resonance absorption, which would lead to the two electron beams as a result of the spherical symmetry of the surface. To check this speculation, we carried out a test experiment in which only the air breakdown was imaged. Figure 4(d) shows a shadowgram of the air breakdown taken at 1 ns produced by a single 2 mJ laser pulse when the water vessel is removed. We can see that most of the laser energy still remains within a 20 μm diam region at a ~ 110 μm distance away from the focus. The area of the defocusing beam is only $\sim 1\%$ of the area of the half spherical density cavity. Therefore, the defocusing light actually irradiates a near-planar critical density surface. This cannot produce the two electron beams symmetrical with the incident laser axis. From Fig. 4(d) we also note that the self-focusing, which may enhance the local laser intensity and the yield of hot electrons, takes place. However, this cannot explain the two peaks of electron emission.

When the following pulses interact with the compressed air and water vapor partially ionized behind the shock wave into air produced by the leading pulse, instabilities may occur in such conditions. However, from the viewpoint of hot electron generation, in principle, the instabilities cannot fully explain the emission direction of hot electrons and their dependence on the incident angle and laser polarization [12].

The generation of nanometer-size and micrometer-size particles by pulsed laser ablation on solid in air have been widely studied [13]. In our experiments, the separation time between pulses is 10 ns. The water droplets can be produced by the first pulse through condensation of water vapor in the ablation plume and direct explosive emission from the focus. Figure 4(e) shows an image of the droplets near the initial water surface taken at 15 ns with a magnification factor of 165. A single pulse with an energy of 2 mJ was used to produce the droplets. We can see the size of the droplets is within 1–6 μm. The average size is about 3 μm. The submicro droplets cannot be observed due to the optical resolution.

To check the electron generation mechanism, we have run 2D particle-in-cell (PIC) simulations. A p-polarized laser pulse with a normalized amplitude $a_0 = 0.1$ and a duration of 50 laser cycles is incident from left normally onto a spherical droplet microplasma with a diameter

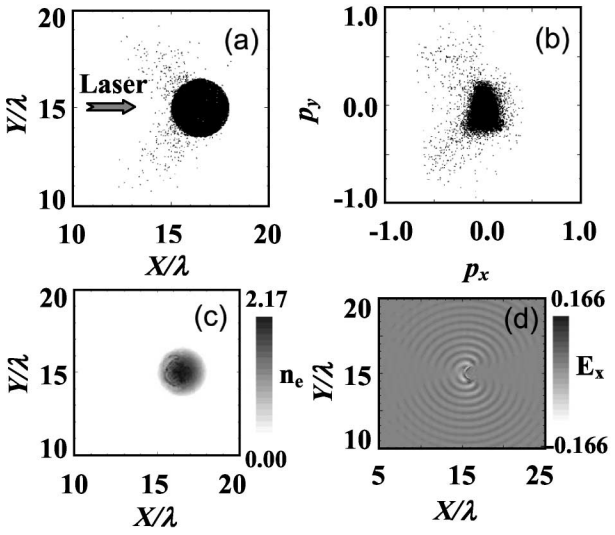

FIG. 5. 2D PIC simulation results for a p-polarized laser pulse at the 40 laser cycle. (a) X-Y plot of electron positions; (b) the distribution of electron momentum in the phase space (p_x, p_y); (c) electron density; and (d) the resonantly excited longitudinal component of the electric field.

of 3λ and a radial density rising parabolically from $0.2n_c$ at the surface to $2n_c$ at the center, where n_c is the critical density. To simplify the problem and save computing time, only one droplet is taken here. However, this does not affect the main interaction physics. Figure 5 shows the distributions of electron positions, momentum, density, and the longitudinal component of the electric field at the 40 laser cycle, respectively. Figures 5(a) and 5(b) show clearly that some of the electrons are accelerated to high energies symmetrically with respect to the laser axis. The ejection angles of most hot electrons are around 40° relative to the laser electric vector. This agrees quite well with the angular distribution measured in experiments. The acceleration mechanism is the resonance absorption occurring at the edge of the microplasma, as judged by the local density increase near the resonant critical surface in Fig. 5(c) and the enhancement of the electrostatic field E_x in Fig. 5(d) (the maximum field of 0.166 is greater than the initial field of $a_0 = 0.1$). On the other hand, no jets of hot electron emission are observed when an s-polarized laser pulse is used. This further proves that resonance absorption is the main mechanism. The fact that there are no jets for an s-polarized laser in the 2D simulations does not contradict our experimental results when the polarization plane is rotated by 90°. In practice, the interaction geometry is three dimensional, where the p-polarized light and s-polarized light is identical for a spherical microplasma.

In the simulations, we find that the ejection angle depends very weakly on the diameter of the droplet microplasma between 2λ and 8λ. This feature remains valid when one adopts different density profiles for the droplet. It shows that the laser field diffraction around the droplet also plays a role, which, combining with the linear mode conversion around the critical surface, is responsible for the two electron jets. No distinct electron jets are observed for droplets with diameter less than λ.

To further confirm the analysis above, an experiment of femtosecond laser direct interaction with water droplets has been performed [14]. The droplets are generated by a gas nozzle with a backed pressure. The droplet size is measured to be ~ 4 μm on average. The diagnostics are the same as the laser-water experiments in air. When a single 2 mJ laser pulse irradiates the droplets in vacuum, we find that the angular distribution of the hot electrons is very similar for both experiments. The results are also shown as the dashed line and circle points in Fig. 3(c) for comparison.

The intrinsically spherical symmetry of the droplets results in the fact that the geometry of the interaction is determined only by the state of the incident laser pulses, even for the case of oblique incidence relative to the water surface. Therefore, the directions of hot electron jets follow the incident laser axis and the electric vector closely whether the laser is obliquely or normally incident and also whether the laser is p polarized or s polarized.

The authors gratefully thank M. Y. Yu and J. X. Ma for useful discussions. This work is supported by the NSFC (Grants No. 10204023, No. 10075075, No. 10105014, and No. 10176034), the K. C. Wang Education Foundation (Hong Kong), the National High-Tech ICF program, and the NKBRSF (Grant No. G199990-75200).

*Author to whom correspondence should be addressed. Email address: jzhang@aphy.iphy.ac.cn

[1] M. Berglund *et al.*, Rev. Sci. Instrum. **69**, 2361 (1998).
[2] J. Noack *et al.*, Appl. Opt. **37**, 4092 (1998).
[3] A. G. Doukas *et al.*, Appl. Phys. B **53**, 237 (1991).
[4] C. D. Ohl *et al.*, Phys. Rev. Lett. **80**, 393 (1998).
[5] O. Baghdassarian *et al.*, Phys. Rev. Lett. **86**, 4934 (2001).
[6] A. Vogel *et al.*, J. Acoust. Soc. Am. **100**, 148 (1996).
[7] P. Zhang *et al.*, Phys. Rev. E **57**, R3746 (1998).
[8] Y. T. Li *et al.*, Phys. Rev. E **64**, 046407 (2001).
[9] J. A. Halbleib *et al.*, ITS 3.0: Integrated TIGER Series of Coupled Electron/Photon Monte Carlo Transport Codes, SAND91-1634, March 1992.
[10] J. P. Christiansen *et al.*, Comput. Phys. Commun. **7**, 271 (1974)
[11] J. Zhang *et al.*, Science **276**, 1097 (1997).
[12] W. L. Kruer, *The Physics of Laser Plasma Interactions* (Addison-Wesley, Redwood City, California, 1988).
[13] C.-B. Juang *et al.*, Appl. Phys. Lett. **65**, 40 (1994); Ching-Bo Juang *et al.*, Appl. Phys. Lett. **65**, 40 (1994); H. Schittenhelm *et al.*, J. Phys. D **29**, 1564 (1996).
[14] T. J. Liang *et al.* (private communication).